PAPER • **OPEN ACCESS**

Analyses of recombination velocities at grain boundaries by cathodoluminescence: control of injection level and effect of grain-boundary inclination angle

To cite this article: Luka Blazevic *et al* 2026 *Nanotechnology* **37** 135703

Nanotechnology

PAPER

OPEN ACCESS

RECEIVED
13 October 2025

REVISED
20 February 2026

ACCEPTED FOR PUBLICATION
18 March 2026

PUBLISHED
1 April 2026

Analyses of recombination velocities at grain boundaries by cathodoluminescence: control of injection level and effect of grain-boundary inclination angle

Luka Blazevic[1], Sebastian Weitz[1], Elisa Artegiani[2], Alessandro Romeo[2], Chang-Yun Song[3], Julia Horstmann[3] and Daniel Abou-Ras[1,*]

[1] Department for Structure and Dynamics of Energy Materials, Helmholtz-Zentrum Berlin für Materialen und Energie GmbH, Berlin 14109, Germany

[2] Laboratory for Photovoltaics and Solid-State Physics (LAPS), Department of Computer Science, University of Verona, Strada le Grazie 15, Verona 37134, Italy

[3] Martin-Luther-University HalleWittenberg, Institute of Physics, Von-Danckelmann-Platz 3, 06120 Halle (Saale), Germany

[*] Author to whom any correspondence should be addressed.

E-mail: daniel.abou-ras@helmholtz-berlin.de

Keywords: cathodoluminescence, grain boundaries, semiconductors, recombination velocity, injection level, inclination angle

Abstract

Cathodoluminescence (CL) analyses of semiconductor materials are routinely employed for the determination of optoelectronic properties. By evaluating CL intensity profiles across grain boundaries (GBs) in polycrystalline semiconductors, the GB recombination velocities can be determined. However, in any CL experiment, control of the injection level is essential, and up to now, there has not been a corresponding, reliable approach. The present work provides such an approach consisting of the analysis of the CL intensity acquired at various beam energies and beam currents, combined with the simulation of the excess-charge carrier density at these beam parameters. It is shown that the CL intensity profiles and therefore, the GB recombination velocities differ strongly when acquiring CL intensities at low and at high injection. Moreover, the present work provides a model for the simulation of CL intensity profiles at GBs, taking into account an inclination angle of the GB with respect to the semiconductor surface. The simulation results show that GB recombination velocities are not affected by the GB inclination angle.

1. Introduction

Cathodoluminescence (CL) in a scanning electron microscope is a standard technique for the optoelectronic analysis of semiconductor materials at the submicrometer scale [1–3]. In polycrystalline thin films with average grain sizes of below 1 μm, CL is, apart from electron-beam-induced current (EBIC) measurements, the only method providing the means of measuring recombination velocities at grain boundaries (GBs) via the evaluation of the CL intensity distributions across these planar defects. As for EBIC analyses, it was shown [4] that recombination velocities of below about 1000 cm s^{-1} cannot be measured reliably by this technique, which is why CL is preferred. The corresponding approach for the determination of recombination velocities at GBs by CL was introduced in [5]. In recent reports, this approach was elaborated further [6] and validated for various photovoltaic absorber materials [6–9]. Most importantly, it is essential to analyze a large number of GBs in one specimen, i.e. at least 15–20, in order to provide good statistics of the measured recombination velocities.

In case the excess charge density generated by the high-energy electron beam during the CL experiment is smaller (larger) than the net-doping density, low-injection (high-injection) conditions are given. Indeed, the description of the recombination velocity at a specific GB depends substantially on the injection level [10]. Therefore, for the correct determination of recombination velocities at GBs in any polycrystalline semiconductor, the injection level needs to be controlled. However, previous studies

on recombination velocities at GBs overlooked this critical aspect [11, 12], and moreover, there is currently no established method for the assessment of the transition range between low-injection and high-injection during CL analyses. In this respect, we note that it is the density of generated electron–hole pairs (number per cm^{-3}) that needs to be determined, not merely their rate (number per s), which can be estimated using various available tools based on Monte-Carlo simulation (e.g. CASINO [13]). And it is indeed the correct assessment of the generation volume which is the most challenging part of the determination of the excess-charge density.

Another aspect also not addressed at all in the determination of recombination velocities via CL analyses is the impact of the inclination angle of the GBs with respect to the specimen surface on the CL intensity distributions across the GBs. In the present work, we provide a combined experimental and simulation approach that can be applied in any CL experiment to determine those beam parameters for a specific semiconductor material that result in low-injection or high-injection conditions. For this approach, the beam energy and beam current need to be varied, and the net-doping density and effective minority-carrier lifetime measured by corresponding analyses. The application of the approach is demonstrated using Cd(Te,Se) thin films [14] with a low net-doping density of about 10^{14} cm^{-3}, for which CL analyses under low-injection conditions are particularly challenging. Further investigations were performed on Ag-containing Cu(In,Ga)Se_2 thin films [15] with a net-doping density on the order of 10^{16} cm^{-3}.

In addition, the present work discusses the impact of the GB inclination with respect to the film surface on the measured recombination velocities. It is shown that although the shape of a CL intensity profile across a GB is affected by the GB inclination angle, the magnitude of the recombination velocity remains independent of the GB geometry.

2. Methods

2.1. Sample preparation

Cd(Te,Se)/CdTe-based devices were fabricated at LAPS, University of Verona, Italy, in a superstrate configuration, with a glass/fluorine-doped tin oxide (FTO)/tin oxide (TO)/Cd(Te,Se)/CdTe/Cu/Au stack. The front contact is a commercial TEC 12D provided by Nippon Sheet Glass-Pilkington, consisting of a FTO/TO bilayer deposited on glass. On this bilayer, a 300 nm-thick CdSe layer, followed by a 300 nm-thick CdTe layer, were deposited by vacuum evaporation at 340 °C, and subsequently annealed in vacuum at 450 °C. An additional 1.4 μm-thick CdTe layer was deposited on the stack and subjected to a $CdCl_2$ activation treatment at 400 °C. This step recrystallized the absorber and formed a $CdSe_xTe_{1-x}$ compound at the front junction. A bromine methanol etching was then applied to remove the $CdCl_2$ residues and to form a Te-rich region on the surface. The back contact was formed by depositing a 1 nm-thick Cu layer and a 30 nm-thick Au layer by vacuum evaporation at room temperature. Finally, the device was annealed at 200 °C to diffuse Cu into the absorber and dope it. Samples fabricated by the described process were previously presented and discussed in detail [16].

The (Ag,Cu)(In,Ga)Se_2 absorber was fabricated at University of Halle, Germany, in a modified 3-stage co-evaporation process on Mo-coated soda-lime glass substrates at temperatures up to 625 °C. Ag was added in the first stage, targeting an [Ag]/([Ag] + [Cu]) ratio of 0.05. In the modified process, Ga was supplied in the second stage to promote the formation of a smoother Ga compositional gradient [17]. The resulting [Ga]/([Ga] + [In]) ratio increases from 0.73 near the front to 0.93 at the back, while the ([Ag] + [Cu])([In] + [Ga]) ratio remained constant at about 0.83. Na was provided by diffusion from the Na-containing soda-lime glass substrates during absorber growth. Additionally, a post-deposition treatment with RbF was applied. To complete the solar cells, a CdS buffer layer was deposited by chemical bath deposition, followed by sputtering i-ZnO/InSnO window layers. As front contact, a Ni/Al/Ni grid was evaporated.

2.2. Material characterization

A Zeiss Merlin scanning electron microscope equipped with a DELMIC SPARC systems was used for acquisition of SEM images and of hyperspectral CL images in the present study. The experiment was conducted at beam energies ranging from 5 to 15 keV and beam currents from 0.5 to 12 nA. Electron backscatter diffraction (EBSD) was performed at 15 keV and 6 nA using a Zeiss UltraPlus scanning electron microscope equipped with an Oxford Instruments Symmetry EBSD detector as well as with the acquisition and evaluation software AZtec. Capacitance–voltage measurements were performed with an HP4284A LCR, using bias frequencies of 10 kHz, 100 kHz and 1 MHz.

The minority carrier lifetime was measured by time-resolved photoluminescence (TRPL) using a diode laser with a wavelength of 640 nm and a repetition rate 2 MHz. The emitted signal was detected by a photomultiplier (H10330A-45, PMA-C). TRPL transients were recorded at room temperature.

3. Brief overview of how to extract recombination velocities from CL analyses

Before discussing the novel insights of the present work concerning the estimation of the injection level as well as the simulation of the CL profiles with varying GB inclination angle, we would like to summarize the basic concepts of the evaluation approach for the recombination velocities extracted from CL intensity distributions across GB planes. The complete description can be found in recent reports [6, 9, 10].

CL profiles are extracted across GBs in CL intensity distributions acquired on polycrystalline thin films. EBSD maps from the same identical areas provide the means to confirm the locations of the GBs as well as to categorize them (e.g. to determine their symmetries). The decrease of the luminescence intensity $I(x)$ from the grain interior (I_{GI}) to the GB plane ($x = 0$) can be simulated using [5]

$$\ln\left(1 - I(x)/I_{\mathrm{GI}}\right) = \ln\left(S/(S+1)\right) - x/L_n, \tag{1}$$

where L_n is the effective diffusion length of minority-charge carriers in the bulk and $S = s_{\mathrm{GB}}\,\tau_{\mathrm{bulk}}/L_n$ is the reduced recombination velocity (unitless) with τ_{bulk} the lifetime of minority-charge carriers in the bulk. Equation (1) is a linear equation that can be fitted easily with the diffusion length L_n as fit parameter. Indeed, τ_{bulk} is very difficult to measure, in contrast to the effective lifetime $\tau_{\mathrm{eff,material}}$, which can be determined via TRPL analysis. Using a simplified version of Matthiessen's rule and assuming a bare, polycrystalline material, the effective lifetime of minority-charge carriers can be approximated by the bulk lifetime and the one at the GB plane (τ_{GB}):

$$\tau_{\mathrm{eff,material}}^{-1} \approx \tau_{\mathrm{bulk}}^{-1} + \tau_{\mathrm{GB}}^{-1}. \tag{2}$$

Note that in equation (2), τ_{bulk} includes recombination at the material surface and (potentially) also at dislocations in the bulk. Finally, the GB lifetime can be expressed as [18]

$$\tau_{\mathrm{GB}} = d_{\mathrm{grain}}/6s_{\mathrm{GB,median}}, \tag{3}$$

where d_{grain} is the median of the grain-size distribution of the polycrystalline material measured by EBSD, and $s_{\mathrm{GB,median}}$ is the median of all s_{GB} values determined at individual GBs. It is easily visible that equations (1)–(3) exhibit an interdependency. The following procedure is used to determine s_{GB} for a specific GB. The bulk lifetime τ_{bulk} is estimated, resulting in a specific τ_{GB} value equation (2). This τ_{bulk} value is used in equation (1) to determine s_{GB}, which again is used in equation (3) to calculate τ_{GB}. The estimation procedure of τ_{bulk} is iterated until the τ_{GB} values from equations (2) and (3) are same (not identical).

The recombination velocity s_{GB} can be described as a function of a prefactor $s_{\mathrm{GB,0}}$ (that represents the nonradiative, Shockley–Read–Hall recombination at the GB plane via corresponding defect states) and the band-bending value, Φ_{GB} [10]:

$$s_{\mathrm{GB}} = s_{\mathrm{GB,0}}\,\exp\left(-\Phi_{\mathrm{GB}}/k_{\mathrm{B}}T\right). \tag{4}$$

For the upward and downward band bending values, we find [10]:

$$\Phi_{\mathrm{GB}}^{\mathrm{up}} = (k_{\mathrm{B}}T)^{0.5} e N_{\mathrm{GB,charge}} / \left[4\left(\varepsilon_0\varepsilon_{\mathrm{r}}N_{\mathrm{A}}\right)^{0.5}\right] \tag{5}$$

and [19]

$$\Phi_{\mathrm{GB}}^{\mathrm{down}} = e^2 N_{\mathrm{GB,charge}}^2 / \left(8\varepsilon_0\varepsilon_{\mathrm{r}}N_{\mathrm{A}}\right), \tag{6}$$

where e is the elemental charge, $N_{\mathrm{GB,charge}}$ is the excess-charge density at the GB plane, ε_0 and ε_{r} are the dielectric permittivities of the vacuum and of the thin-film material, and N_{A} is the net-doping density of the semiconductor. Note that a result of the derivation of equation (4) [10] is that band-bending value, Φ_{GB}, is limited to an interval between about −100 and +100 meV. Since the band bending is a result of an effective redistribution of the free charge carriers (electrons and holes) in a semiconductor,

at room temperature, the absolute value of Φ_{GB} is relevant (i.e. $\Phi_{GB} > k_B T$) only if the net-doping density is sufficiently large (typically larger than about 1×10^{14} cm^{-3}) [19]; moreover, the band-bending value decreases again for very high net-doping densities [19]. When determining numerous s_{GB} values at various GBs in a polycrystalline semiconductor with corresponding net-doping density, these values range across two to four orders of magnitude. This behavior can be explained by equation (4). The prefactor $s_{GB,0}$ changes slightly from GB to GB, while the band-bending value, Φ_{GB}, even if varying slightly between about −100 and +100 meV, represents a strong lever on the recombination velocity s_{GB} via the exponential function.

We note that equation (4) is only valid for semiconductors analyzed under low-injection conditions. The equation for high-injection conditions is different [10]:

$$s_{GB} = N_{GB,recomb} v_{th} \left(\sigma_{GB,p}^{-1} + \sigma_{GB,n}^{-1} \right), \tag{7}$$

where $N_{GB,recomb}$ is the effective defect density at GBs connected with the nonradiative recombination, ${\sigma_{GB,p}}^{-1}$ and $\sigma_{GB,n}$ are the corresponding capture cross-sections for holes and electrons, and v_{th} is the thermal velocity for holes and electrons (which we assume to be the same). The different forms of equations (4) and (7) show that it is essential to control the injection level during the CL experiment.

4. Results

4.1. Microstructure and minority-charge carrier lifetimes in the Cd(Te,Se) and (Ag,Cu)(In,Ga)Se$_2$ absorber layers

The Cd(Te,Se) and (Ag,Cu)(In,Ga)Se$_2$ solar cells analyzed in the present work consist of glass/FTO/TO/Cd(Te,Se)/Cu/Au and InSnO/i-ZnO/CdS/(Ag,Cu)(In,Ga)Se$_2$/Mo/glass stacks (figures 1(a) and (c)). In figures 1(b) and (d), the EBSD orientation-distribution maps (orientations perpendicular to the substrate, given as false colors, see legends) are depicted. The average grain sizes in the Cd(Te,Se) and (Ag,Cu)(In,Ga)Se$_2$ are about 0.6 and 1.2 μm.

TRPL transients acquired on the Cd(Te,Se) and (Ag,Cu)(In,Ga)Se$_2$ absorber layers are shown in figure 2. These transients were fitted using biexponential functions to determine the effective minority-charge carrier (electron) lifetimes of $\tau_{eff} = 3$ ns for Cd(Te,Se) and $\tau_{eff} = 3$ ns for (Ag,Cu)(In,Ga)Se$_2$.

4.2. Assessment of the injection level

The CL intensity, i.e. the number of luminescence photons emitted from a material per second and area, is very closely linked to the injection level. This is not astonishing, considering that the luminescence emission from a semiconductor is a result of the radiative recombination of excited charge carriers. In a CL experiment, their concentration can be controlled via the beam energy and the beam current. In case the concentration of the electron–hole pairs excited by the electron beam is smaller than the net-doping density of the semiconductor, low injection is given, and else, high injection.

It was reported by Rao-Sahib and Wittry [20] that the CL intensity I_{CL} measured on p-type GaAs crystals varies in a superlinear manner with the beam current I_B, i.e. $I_{CL} \propto {I_B}^m$, where m is a factor being dependent on I_B as well as on the beam energy E_B and varying between 1 and 2. Guthrey and Moseley [21] suggested that this factor m may be used to estimate the injection level for a specific beam current and energy: for m between 1 and 2, a mixture of low-injection and high-injection conditions is given, while $m = 1$ is identical with high-injection condition. We tried to apply this approach to the CL intensities I_{CL} measured at various I_B and E_B values; however, the expected trend with a large slope m decreasing towards $m = 1$ for increasing I_B was not found for any of the beam energies E_B.

Therefore, we suggest a different approach to estimate the injection level for any electron-beam experiment conducted on a semiconductor. The bottom line is the fact that radiative recombination rate R_{rad}, which is proportional to the CL intensity, can be expressed as

$$R_{rad} = B(np - n_0 p_0) \approx Bnp, \tag{8}$$

where B is the material-specific radiative recombination coefficient, n and p are the electron and hole concentrations in the excited state, and n_0 and p_0 are these concentrations in the thermodynamic equilibrium. As long as the CL experiment is conducted under low-injection conditions, n is by at least one order of magnitude smaller (larger) than p in a p-type (n-type) semiconductor. In case of high injection, n is equal to p, i.e. R_{rad} and thus, the CL intensity, become very large.

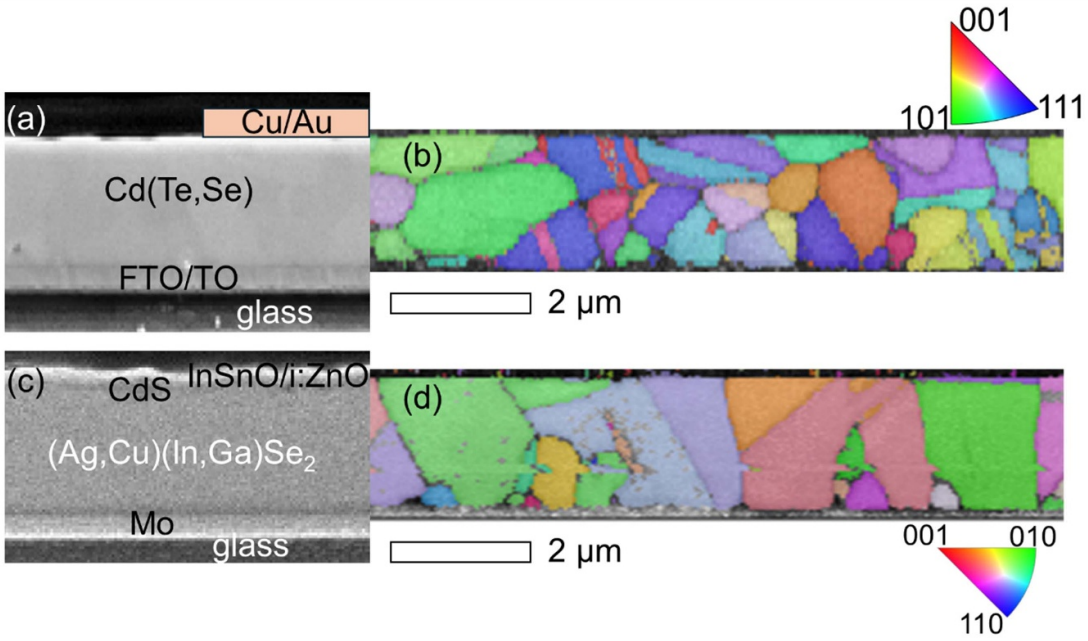

Figure 1. (a) and (c): Cross-sectional SEM images of the glass/FTO/TO/Cd(Te,Se)/Cu/Au and InSnO/i-ZnO/CdS/(Ag,Cu)(In,Ga)Se_2/Mo/glass solar-cell stacks analyzed in the present work. (b) and (d): EBSD orientation-distribution maps acquired on the same cross-sectional specimens as in (a) and (c). The local orientations perpendicular to the substrate are given as false colors, see the legends.

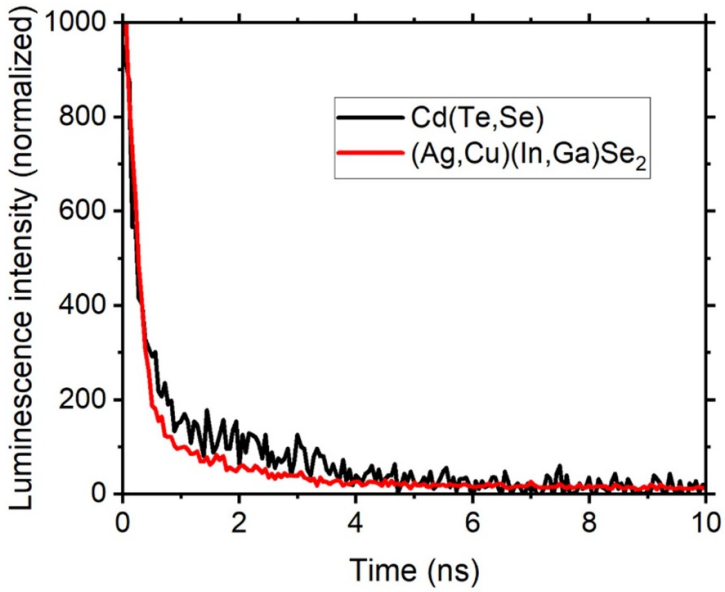

Figure 2. TRPL transients acquired on the Cd(Te,Se) (black solid line) and (Ag,Cu)(In,Ga)Se_2 absorber layers (red solid line). The corresponding effective minority-charge carrier (electron) lifetimes were determined to $\tau_{eff} = 3$ ns for Cd(Te,Se) and $\tau_{eff} = 3$ ns for (Ag,Cu)(In,Ga)Se_2 using a biexponential fitting routine.

Thus, in a CL experiment, it is possible to detect the transition between low-injection and high-injection conditions by a strong increase in the CL intensity. For this approach, the beam current was increased from small to high values for various beam energies. The CL emission rates (in counts/s) were determined by acquiring CL spectra on individual spots on the semiconductor specimen (it was not possible to control whether it was positioned in the grain interiors), by integrating these spectra, and by dividing the resulting number of counts by the acquisition duration. The CL spectra were measured at different positions on the cross-section in order to avoid influences of carbon contamination on the cross-section surface.

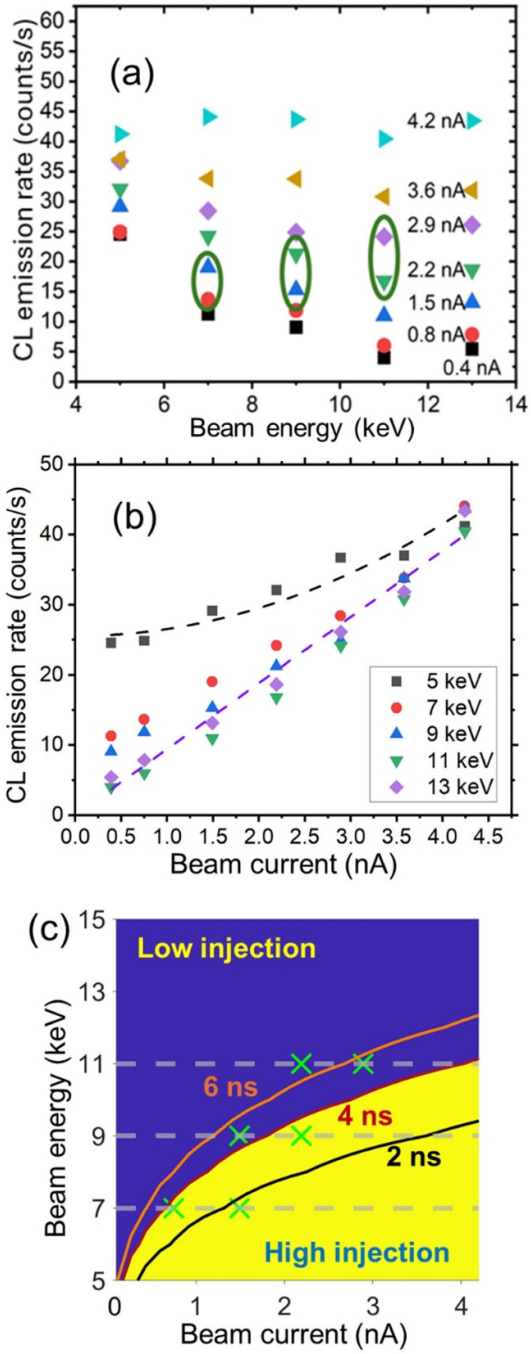

Figure 3. (a) Integrated CL emission rate from the Cd(Te,Se) thin film as a function of the beam current for various beam energies. Green ovals indicate the points interpreted as transitions from low to high injection. (b) Integrated CL emission rate plotted versus the beam current for various beam energies. The dashed lines are parabolic (function $y(x) = A + x^2$, with A as fit parameter) and linear fits to the data acquired at 5 and 13 keV. (c) Distribution of the regimes for low and high injection, estimated using equation (9), $N_A = 3 \times 10^{14}$ cm^{-3} and $\tau_{bulk} = 4$ ns, depicted for various beam-current/beam-energy pairs. The green crosses highlight the current values marked by green ovals in (a). When assuming an error of the bulk lifetime of ± 2 ns, in order to account for inaccuracies of the approach, all current value pairs are separated by any of the threshold lines.

Figure 3(a) shows the CL emission rates obtained at different beam currents and beam energies acquired on a cross-sectional specimen of the Cd(Te,Se) thin-film (net-doping density of 3×10^{14} cm^{-3}). As expected, the CL emission rate increases with increasing beam current for all beam energies ranging from 5 to 13 keV. Between the current values highlighted by green ovals, these increases are particularly strong, suggesting transitions from low-injection to high-injection conditions. However, it remains ambiguous whether the highlighted beam-current pairs indeed indicate the transition between the injection regimes correctly or not, since also other, likewise strong increases in CL intensity are visible in the viewgraph.

A different way of checking the injection level during the electron-beam experiment in a specific material is to introduce the excess charge-carrier density Δn in equation (8). For the electron and hole densities in a p-type semiconductor, we can write $n = n_0 + \Delta n \approx \Delta n$ and $p = p_0 + \Delta p = p_0 + \Delta n$. The radiative recombination rate R_{rad} and thus, the CL intensity I_{CL}, is (equation (8)) proportional to $\Delta n\ (p_0 + \Delta n)$. For low-injection conditions, p_0 is substantially larger than Δn, i.e. I_{CL} is proportional to $\Delta n\, p_0$ and thus, to Δn. For high-injection conditions, Δn is substantially larger than p_0, i.e. I_{CL} is proportional to $(\Delta n)^2$. The excess charge-carrier density Δn generated by an electron beam with beam energy E_B and beam current I_B can be expressed by [22]

$$\Delta n = E_B I_B\,(1-\Lambda)\,/\left[(eE_{eh})\,4/3\pi\,(R/2)^3\right] \times \tau_{bulk}, \tag{9}$$

where e is the elemental charge, E_{eh} is the effective energy necessary to form an electron–hole pair, $E_{eh} = 2.1\ E_{gap} + 1.2$ eV (E_{gap} is the band-gap energy of the semiconductor), Λ is the material-specific backscatter coefficient with $\Lambda = (\alpha - 1 + (0.5)^{\alpha})/(\alpha + 1)$ and $\alpha = 0.045Z$ (Z is the average atomic number), R is the range of the electron beam penetrating into the material, and τ_{bulk} is the bulk lifetime already discussed in equations (1) and (2); we discuss the unambiguous determination of τ_{bulk} further below.

From equation (9), it is apparent that the excess charge-carrier density Δn is proportional to the beam current I_B. Consequently, the CL intensity I_{CL} should be proportional to the beam current I_B for low-injection and to $(I_B)^2$ for high-injection conditions. This relationship is visualized in figure 3(b). For a low (high) beam energy of 5 keV (13 keV), the dependency I_{CL} vs. I_B can be fitted successfully by a parabolic (linear) fit (dashed lines in figure 3(b)). However, for the beam energies of 7, 9, and 11 keV, it is not possible to identify unambiguously the transition from low-injection to high-injection conditions by a change from linear to parabolic dependency in the I_{CL} vs. I_B plots.

Therefore, we need to confirm the transitions between the injection regimes by simulation. We assess the excitation volume $4\pi/3 \times (R/2)^3$ in equation (9) by assuming a sphere with a diameter equal to the electron range R. This quantity is indeed a critical parameter in the estimate of Δn. There are various equations reported in the literature that describe the electron-penetration range R, i.e. the Gruen range [23], the universal curve of Everhart and Hoff [24], and the maximum range of Kanaya and Okayama [25] (see the overview by Kurniawan and Ong [26]). We tested all of them and found that using the electron range of Kanaya and Okayama, the agreement between simulated and experimental transitions from low to high injection is best. This maximum electron range R_{K-O} can be calculated by [25]

$$R_{K\text{-}O} = 2.76 \times 10^{-11}\, A\, E_B^{5/3}\left(1 + 0.978 \times 10^{-6} E_B\right)^{5/3} / \left[\rho\, Z^{8/9}\ \left(1 + 1.957 \times 10^{-6} E_B\right)^{4/3}\right] \tag{10}$$

where A is the average atomic weight and ρ is the mass density of the semiconductor.

The bulk lifetime τ_{bulk} within individual grains in a polycrystalline semiconductor is generally very difficult to assess, in contrast to the effective minority-charge carrier lifetime τ_{eff} in a semiconductor. We found the following approach for the assessment of τ_{bulk} feasible. As a first step, we set τ_{eff} to τ_{bulk} in equation (9). We calculated the excess charge-carrier density Δn considering an electron beam impinging in Cd(Te,Se) for various beam currents and energies using equation (9) and, comparing Δn with the net doping density N_A (3×10^{14} cm^{-3} for Cd(Te,Se)), determined the threshold line between the low-injection ($\Delta n < N_A$) and high-injection ($\Delta n \geqslant N_A$) regimes. Next, we increased the lifetime value in equation (9) (assuming $\tau_{bulk} > \tau_{eff}$). At a specific τ_{bulk} value, 4 ns, the current pairs highlighted by circles in figure 4(a), indicating the transition between low and high injection, were, for a beam energy of 9 keV, separated by the threshold line (figure 3(c)).

In the present work, we confirmed this τ_{bulk} value of 4 ns via the approach described in section 3 above (applying equation (2)), using CL data acquired at 9 keV (shown in section 4.3). However, for beam energies of 7 and 11 keV, the current pairs (highlighted by circles in figure 3(a)) were not separated by the same threshold line. We solved this discrepancy by considering an error bar of this τ_{bulk} value of ± 2 ns. The resulting threshold lines separated the current pairs at 7 and 11 keV. This result shows that it is appropriate to assume an error of the τ_{bulk} value of about 30%–50%. At 5/13 keV, high/low injection was found for any beam current, which agrees well with the experimental findings in figures 3(**a**) and (b). From the results shown in figure 3(c), it became apparent that the transition between the injection regimes is not sharp but rather gradual. We can expect that this approach becomes more accurate for a larger number of beam energies at which the beam current is varied.

We applied the approach to estimate the injection level also to a CL analysis of the (Ag,Cu)(In,Ga)Se_2 layer (shown in section 4.3) with a net-doping density of $N_A = 1 \times 10^{16}$ cm^{-3}. The corresponding results are shown in figures 4(a)–(c). At 11 and 13 keV, all beam current values of up to

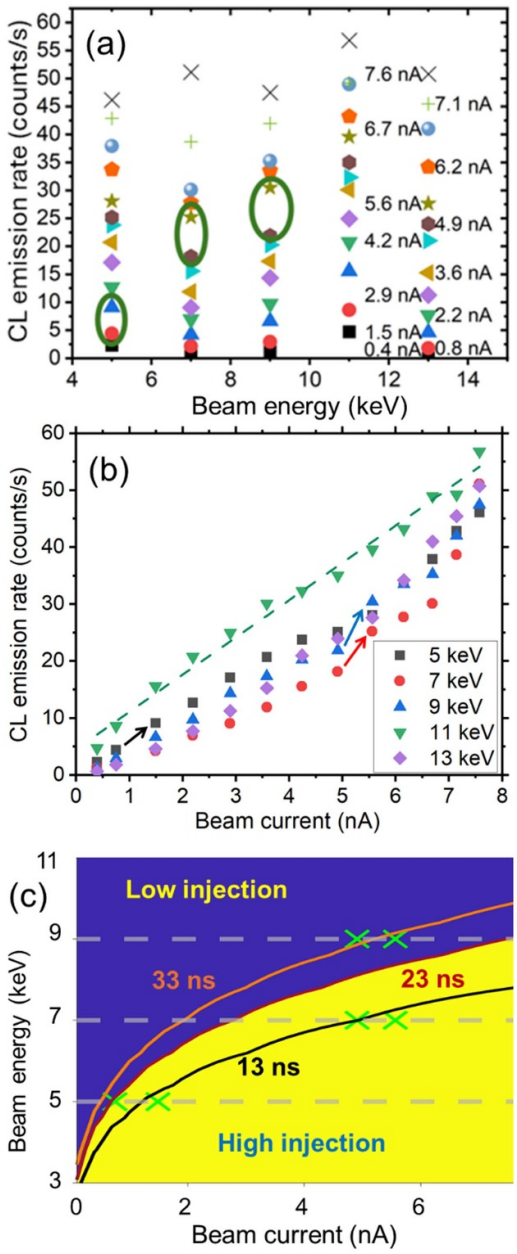

Figure 4. (a) Integrated CL emission rate from the (Ag,Cu)(In,Ga)Se_2 thin film as a function of the beam current for various beam energies. Green ovals highlight the measurement points indicating transitions from low to high injection. (b) Integrated CL emission rate plotted versus the beam current for various beam energies. The dashed line is a linear fit to the data acquired at 11 keV. Black, red, and blue arrows highlight the measurement points indicating transitions from low to high injection. (c) Distribution of the regimes for low and high injection, estimated using equation (9), $N_A = 1 \times 10^{16}$ cm^{-3} and $\tau_{bulk} = 23$ ns, depicted for various beam-current/beam-energy pairs. The green crosses highlight the current values marked by green ovals in (a). When assuming an error of the bulk lifetime of ± 10 ns, all current value pairs are separated by any of the threshold lines.

almost 8 nA resulted in low-injection conditions. In contrast, using 5, 7, and 9 keV, the CL emission rates in figure 4(a) exhibit strong increases between the current values highlighted by the green ovals. In figure 4(b), depicting the CL emission rates vs. the beam current (as in figure 3(b)), these strong increases are also visible (highlighted by arrows). The current values between which strong increases occur are separated by one of the threshold lines in figure 4(c) assuming a bulk lifetime of 23 $\pm$ 10 ns. Also for this sample, we confirmed this bulk lifetime at 9 keV via the approach described in section 3 above (applying equation (2)). Table 1 provides all input parameters for equations (9) and (10) used for the polycrystalline Cd(Te,Se) and (Ag,Cu)(In,Ga)Se_2 thin films.

Table 1. Material parameters used in equations (9) and (10) for the simulations shown in figures 3(**c**) and 4(c).

Parameter	Cd(Te,Se)	$(Ag,Cu)(In,Ga)Se_2$
E_{gap} (eV)	1.4	1.15
Z	50	33
τ_{bulk} (ns)	4	23
A	120.01	76.47
ρ (g cm^{-3})	5.85	5.60
N_A (cm^{-3})	3×10^{14}	1×10^{16}

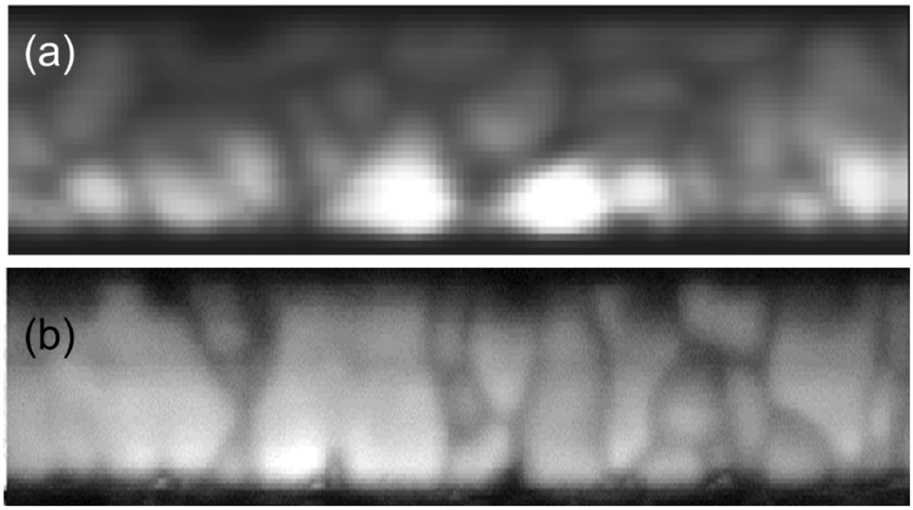

Figure 5. CL intensity distributions acquired under low-injection conditions on the same cross-sectional specimens of the Cd(Te,Se) (a) and for the $(Ag,Cu)(In,Ga)Se_2$ solar cell (b) as in the SEM images and EBSD maps shown in figure 1. The absorber-layer thicknesses are correspondingly about 2−2.5 μm.

4.3. CL intensity profiles across GBs for low and high injection

Since we are now able to acquire CL profiles across GBs in a polycrystalline semiconductor under controlled injection conditions, it is interesting to compare corresponding CL data acquired in the low-injection and high-injection regime. Figure 5 gives the CL intensity distributions acquired at 9 keV under low-injection conditions (1 nA for Cd(Te,Se), 0.5 nA for $(Ag,Cu)(In,Ga)Se_2$) on the same cross-sectional specimens as for the SEM images and EBSD maps shown in figure 1. The CL intensity is decreased at GBs owing to enhanced nonradiative recombination. By applying the approach described in section 3, recombination velocities s_{GB} were determined for a large number of GBs in the Cd(Te,Se) and $(Ag,Cu)(In,Ga)Se_2$ thin films under low-injection and high injection conditions (figure 6). Independent of the material and of the injection condition, the s_{GB} values range over several orders of magnitude (the reason for this behavior is provided in [10]). The medians of the s_{GB} values are highlighted by white bars. These median values are substantially larger for the s_{GB} values obtained under high-injection conditions.

Figure 7 shows normalized CL profiles across GBs acquired on the polycrystalline Cd(Te,Se) (figure 7(a)) and $(Ag,Cu)(In,Ga)Se_2$ (figure 7(b)) thin films at a beam energy of 9 keV and at various beam currents (1 and 4 nA for Cd(Te,Se) as well as 0.5 and 10 nA for $(Ag,Cu)(In,Ga)Se_2$). The profiles given in figures 7(**a**) and (b) were each acquired at the identical GB (only under different injection conditions). For better comparison, the CL intensities were normalized to 1. It is apparent that the difference in CL intensity between grain interiors and GB is much larger in the case of high injection. Correspondingly, the recombination velocities determined at these GBs are substantially different under low-injection (210 cm s^{-1} in figure 7(a) vs. 1880 cm s^{-1} in figure 7(b)) and high-injection conditions (5450 cm s^{-1} in figure 7(a) vs. 3500 cm s^{-1} in figure 7(b)). Similarly high recombination velocities in polycrystalline CdTe thin films were reported by Kanevce *et al* [11] and by Stechmann *et al* [12], who conducted the CL experiments at too high beam currents. This result highlights again the importance of controlling the injection level in CL experiments.

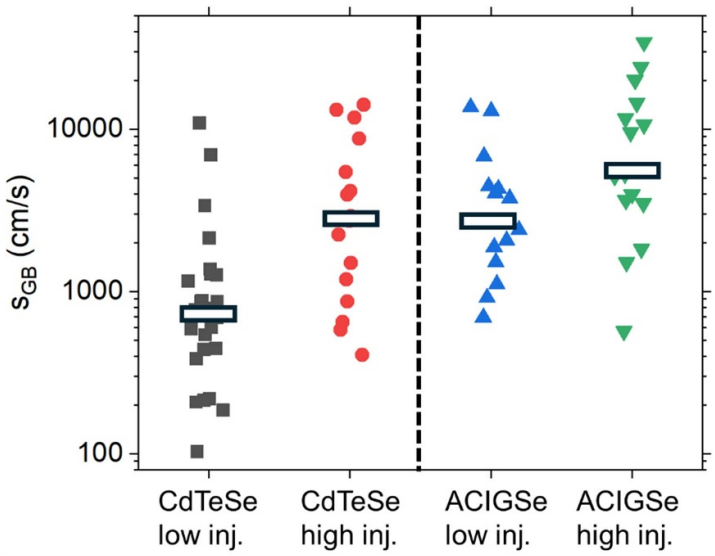

Figure 6. Recombination velocities s_{GB} determined by the approach described in section 3, using CL intensity maps acquired at a beam energy of 9 keV and at beam currents of 1 (low injection) and 4 nA (high injection) for Cd(Te,Se) as well as of 0.5 (low injection) and 10 nA (high injection) for (Ag,Cu)(In,Ga)Se_2 (ACIGSe). Their medians are highlighted by white bars. These median values are substantially larger for the s_{GB} values obtained under high-injection conditions.

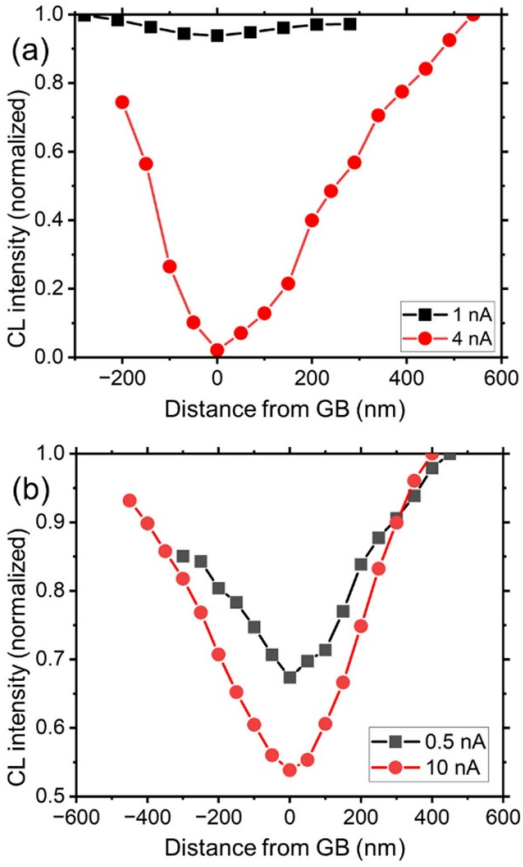

Figure 7. (a) Normalized CL intensity profiles across GBs in (a) a Cd(Te,Se) and (b) a (Ag,Cu)(In,Ga)Se_2 thin film acquired at 9 keV each under low-injection (1 nA, 0.5 nA) and high-injection conditions (4 nA, 10 nA). In each film, the identical GB was analyzed under different injection conditions. From the results depicted in figures 3 and 4, the injection levels at these beam parameters can be confirmed. At high injection, the difference in CL intensity between grain interiors and GB is much larger than at low injection.

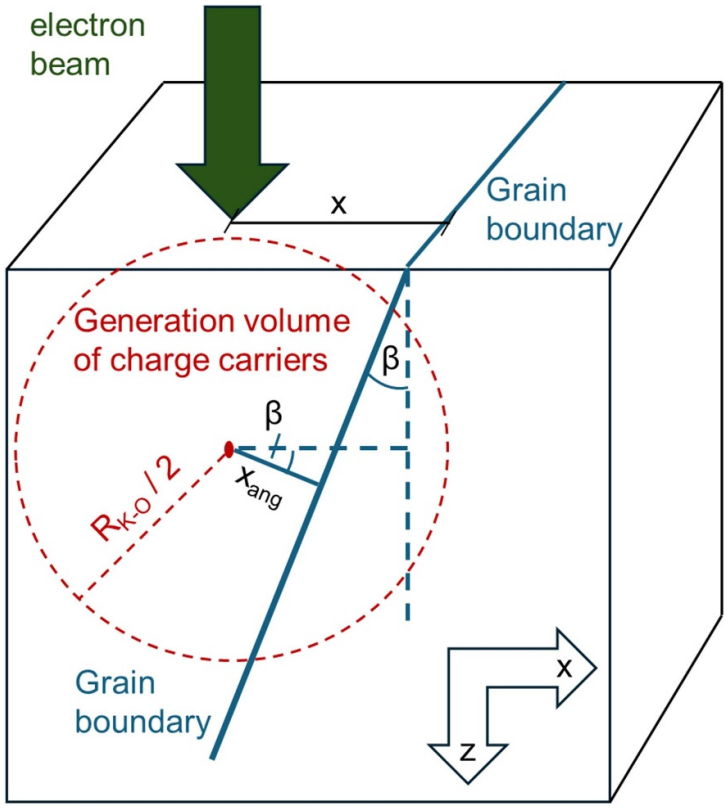

Figure 8. Schematic illustration of a tilted GB within the material and charge-carrier generation by the electron beam. The excitation volume is approximated by a sphere with diameter equal to the electron-penetration range $R_{K–O}$ (equation (10)). The distance of a generated charge carrier to the GB plane at an inclination angle of $\beta = 0$ degrees is expressed by the coordinate x, with $x \leqslant R_{K–O}$. This coordinate x becomes smaller, x_{ang}, for increasing inclination angles $\beta > 0$.

4.4. Influence of the inclination angle at the GB plane on the CL signal

So far, we have assumed that the GB plane is oriented perpendicular to the specimen surface. However, in real microstructures, GBs can exhibit various inclination angles with respect to the surface, potentially influencing the intensity profiles. To investigate this effect, simulations were performed for GBs with varying tilt angles. A schematical drawing of the generation of charge carriers near a tilted GB plane is shown in figure 8. Correspondingly, the excitation volume of the incident electron beam in a semiconductor can be estimated by a sphere with diameter equal to the electron-penetration range $R_{K–O}$ (equation (9) and 10). The distance of a generated charge carrier to the GB plane at an inclination angle of $\beta = 0$ degrees is expressed by the coordinate x, with $x \leqslant R_{K–O}$. This coordinate x becomes smaller for increasing inclination angles:

$$x_{ang} = x\cos(\beta) - R_{K\text{-}O}/2 \times \sin(\beta).$$

We assume that in the presence of a GB, the density of the excess-charge carriers generated by the electron beam is decreased by the enhanced, nonradiative recombination at the GB plane. A corresponding equation describing this reduced excess charge-carrier density was proposed by Hackett [27] when dealing with generation of charge carriers close to the surface in a semiconductor:

$$\Delta n_{red} = (G_0 L_n)/(2D_n) \times \left[\exp\left(-\left|x_{ang} - R_{K\text{-}O}/2\right|/L_n\right) + ((1-S)/(1+S)) \times \exp\left(-\left|x_{ang} + R_{K\text{-}O}/2\right|/L_n\right)\right]. \quad (11)$$

Here, $G_0 = E_B I_B/(e\,E_{eh}) \times (1 - \Lambda)$ (see equation 9), D_n is the diffusion constant of the minority-charge carriers in the semiconductor, and L_n and S are the same quantities already introduced in equation (1). At low-injection conditions, we can assume that the CL intensity is proportional to Δn_{red} decreased by the nonradiative recombination in the bulk and at the film surface. In the following, we will regard the relative change in CL intensity between grain interiors and GB plane. Thus, we will put $\Delta n_{red} = 1$ in the grain interior far away from the GB plane (which is positioned at $x_{ang} = 0$), and x_{ang} runs only between $x_{ang} = 0$ and the x_{ang} value at $\Delta n_{red} = 1$. Considering that the nonradiative recombination in the bulk

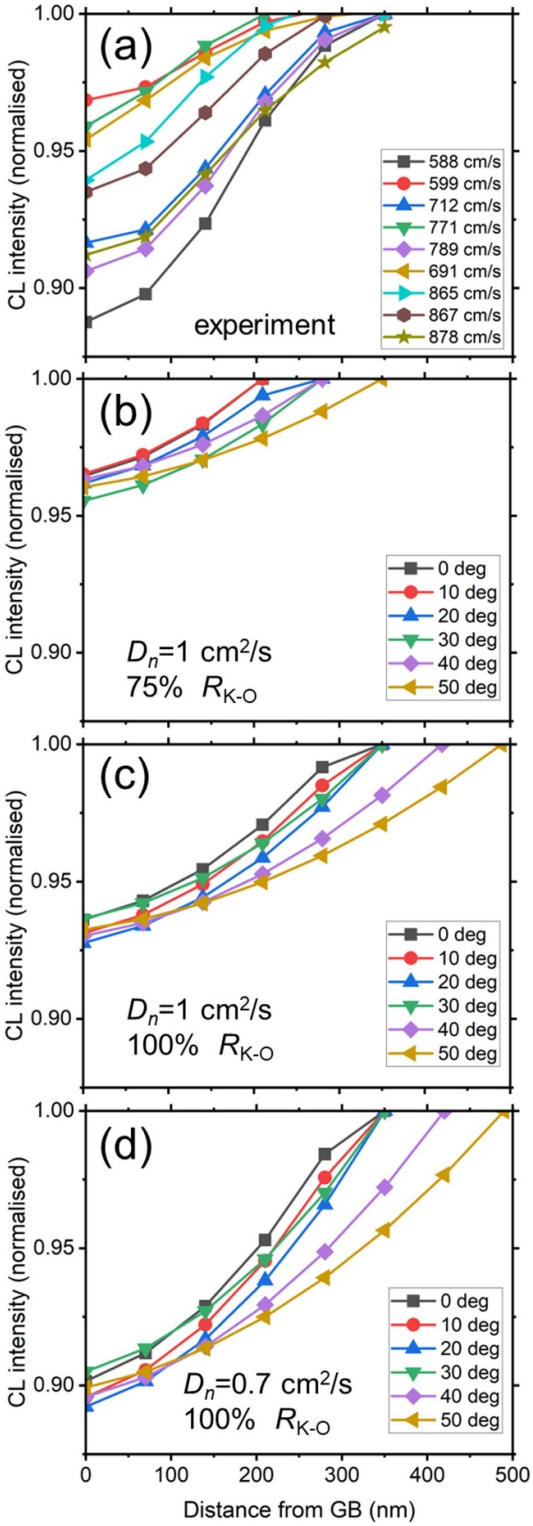

Figure 9. (a) Experimental CL intensity profiles across GBs in a Cd(Te,Se) thin film with similar recombination velocities ranging from 600 to 900 cm s^{-1}, extracted from the intensity distribution map acquired at beam energy of E_B = 9 keV and a beam current of I_B = 1 nA. (b)–(d) Intensity profiles simulated using equation (11) and assuming slightly different diffusion constants (0.7 and 1 cm^2 s^{-1}) and electron-penetration depths (75% and 100% R_{K-O}), i.e. excitation volumes.

and at the film surface is the same for all x_{ang}, the normalized CL intensity profiles can be simulated simply using Δn_{red} (x_{ang}) (equation (11)). Since in our CL experiments, we use rather low beam energies of 9 keV, we simplify the simulation of the CL intensity profiles by assuming a delta function for the generation profile of the electron beam (instead of convoluting Δn_{red} with a generation profile in the simulation that depends on the beam energy).

We found that while the CL intensity contrast at the GB (i.e. the intensity difference between grain interior and GB) changes substantially for various GB inclination angles $\beta>0$ (see figure 9), the measured recombination velocities s_{GB} remain unaffected. This is because s_{GB} is not determined directly from the CL intensity contrast, but via equation (1), which includes also further quantities.

In order to demonstrate the application of the model described by equation (11), we simulated CL intensity profiles across GBs in a polycrystalline, *p*-type Cd(Te,Se) thin film, acquired at a beam energy of $E_B = 9$ keV and a beam current of $I_B = 1$ nA (figure 9). These profiles were selected since the corresponding recombination velocities s_{GB} exhibit similar values ranging from 600 to 900 cm s^{-1}. Apparently, despite the similar s_{GB}, the CL intensity contrast at the GB is substantially different. We found that the diffusion constant D_n strongly affects the CL intensity contrast in the simulated CL intensity profiles, while via the electron-penetration range R_{K-O}, the width of the profile (distance between $x_{ang} = 0$ and x_{ang} for which the normalized CL intensity is 1) can be effectively varied. Rather minor impact has the bulk lifetime and the recombination velocity. All experimental CL intensity profiles (figure 9(a)) can be simulated successfully for β ranging from 0 to 50 degrees assuming slight variations in the diffusion constant D_n (about 0.7–1 cm^2 s^{-1}, in good agreement with literature values reporting 0.1–1 cm^2 s^{-1}, order of magnitude [28, 29] as well as in the electron-penetration range R_{K-O} (about 75%–100%) (figures 9(b)–(d)). These slight variations are appropriate; the diffusion constant D_n or, via Einstein's relation $eD_n = \mu_n k_B T$, also the electron mobility μ_n, can be expected to vary slightly between neighboring grains. And as already discussed above, the estimate of the excitation volume as sphere with diameter equal to R_{K-O} exhibits a substantial error (75% of R_{K-O} results in a smaller excitation volume by a factor of about 2.3).

5. Conclusions

The present work describes how the injection level in any CL analysis of a semiconducting material can be controlled by combining the CL intensity acquired at various beam energies and beam currents with a simple model calculating the excess-charge carrier density. The substantial effect of the injection level on CL intensity profiles across GBs in photovoltaic absorber materials was demonstrated. By evaluation of these intensity profiles, the recombination velocities at the GBs can be determined. Moreover, it was shown that the inclination of a GB plane with respect to the semiconductor surface does not affect the recombination velocity calculated via the presented model.

Acknowledgments

L B and D A are grateful for support by the German-Israeli Helmholtz International Research School HI-SCORE (HIRS-0008). This work has received funding from the European Union's Horizon Europe research and innovation program under Grant Agreement No. 101122203 (project Hi-BITS). Special thanks are due to Reviewer #3, Editorial Board member of Nanotechnology, for the suggestions that helped to improve the quality of the present work.

Data availability statement

All data that support the findings of this study are included within the article. The raw data of all results shown in the present work are available with the corresponding author upon reasonable request.

Author contributions

Luka Blazevic 0009-0004-9338-6658
Data curation (lead), Investigation (lead), Writing – original draft (equal)

References

[1] Yacobi B G and Holt D B 1990 *Cathodoluminescence Microscopy of Inorganic Solids* (Springer)
[2] Coenen T and Haegel N M 2017 *Appl. Phys. Rev.* **4** 031103
[3] Dang Z, Chen Y and Fang Z 2023 *ACS Nano* **17** 24431

[4] Nichterwitz M, Abou-Ras D, Sakurai K, Bundesmann J, Unold T, Scheer R and Schock H W 2009 *Thin Solid Films* **517** 2554
[5] Mendis B G, Bowen L and Jiang Q Z 2010 *Appl. Phys. Lett.* **97** 092112
[6] Quirk J, Rothmann M, Li W, Abou-Ras D and McKenna K P 2024 *Appl. Phys. Rev.* **11** 011308
[7] Thomas S, Witte W, Hariskos D, Gutzler R, Paetel S, Song C-Y, Kempa H, Maiberg M and Abou-Ras D 2024 *Prog. Photovolt. Res. Appl.* **32** 930
[8] Thomas S, Witte W, Hariskos D, Paetel S, Song C-Y, Kempa H, Maiberg M, El-Ganainy N and Abou-Ras D 2025 *Prog. Photovolt. Res. Appl.* **33** 265
[9] Abou-Ras D, Weitz S, Huang J, Sun K, Gong Y, Jimenez-Arguijo A, Dimitrievska M, Hao X and Saucedo E 2025 *Energy Environ. Mater.* **8** e70048
[10] Abou-Ras D and Maiberg M 2025 *J. Appl. Phys.* **137** 233106
[11] Kanevce A, Moseley J, Al-Jassim M and Metzger W K 2015 *IEEE J. Photovolt.* **5** 1722
[12] Stechmann G, Zaefferer S, Schwarz T, Konijnenberg P, Raabe D, Gretener C, Kranz L, Perrenoud J, Buecheler S and Tiwari A N 2017 *Sol. Energy Mater. Sol. Cells* **166** 108
[13] Drouin D, Couture A R, Joly D, Tastet X, Aimez V and Gauvin R 2007 *Scanning* **29** 92
[14] Lingg M, Buecheler S and Tiwari A N 2019 *Coatings* **9** 520
[15] Keller J, Kiselman K, Donzel-Gargand O, Martin N M, Babucci M, Lundberg O, Wallin E, Stolt L and Edoff M 2024 *Nat. Energy* **9** 467
[16] Artegiani E, Gasparotto A, Meneghini M, Meneghesso G and Romeo A 2023 *Sol. Energy* **260** 11
[17] Zahedi-Azad S, Maiberg M and Scheer R 2020 *Prog. Photovolt. Res. Appl.* **28** 1146
[18] Li J *et al* 2022 *Nat. Energy* **7** 754
[19] Seto J Y W 1975 *J. Appl. Phys.* **46** 5247
[20] Rao-Sahib T S and Wittry D B 1969 *J. Appl. Phys.* **40** 3745
[21] Guthrey H and Moseley J 2020 *Adv. Energy Mater.* **10** 1903840
[22] Abou-Ras D and Kirchartz T 2019 *ACS Appl. Energy Mater.* **2** 6127
[23] Grün A E 1957 *Z. Naturforsch. A* **12** 89
[24] Everhart T E and Hoff P H 1971 *J. Appl. Phys.* **42** 5837
[25] Kanaya K and Okayama S 1972 *J. Phys. D: Appl. Phys.* **5** 43–58
[26] Kurniawan O and Ong V K S 2007 *Scanning* **29** 280
[27] Hackett W H 1972 *J. Appl. Phys.* **43** 1649
[28] Toušek J, Toušková J and Křivka I 2024 *Sci. Rep.* **14** 899
[29] Kuciauskas D, Moseley J, Ščajev P and Albin D 2020 *Phys. Status Solidi RRL* **14** 1900606